

# The transition from carbon dust to silicates production in low-metallicity AGB and SAGB stars

P. Ventura,<sup>1</sup> M. Di Criscienzo,<sup>1</sup> R. Schneider,<sup>1</sup> R. Carini,<sup>1,2</sup> R. Valiante,<sup>1,3</sup>  
F. D’Antona,<sup>1</sup> S. Gallerani,<sup>1</sup> R. Maiolino,<sup>1</sup> A. Tornambé<sup>1</sup>

<sup>1</sup>*INAF – Osservatorio Astronomico di Roma, Via Frascati 33, 00040, Monte Porzio Catone (RM), Italy*

<sup>2</sup>*Dipartimento di Fisica, Università di Roma “La Sapienza”, P.le Aldo Moro 5, 00143, Roma, Italy*

<sup>3</sup>*INAF – Osservatorio Astrofisico di Arcetri, Largo Enrico Fermi 5, 50125 Firenze, Italy*

Accepted, Received; in original form

## ABSTRACT

We compute the mass and composition of dust produced by stars with masses in the range  $1M_{\odot} \leq M \leq 8M_{\odot}$  and with a metallicity of  $Z = 0.001$  during their AGB and Super AGB phases. Stellar evolution is followed from the pre-main sequence phase using the code ATON which provides, at each timestep, the thermodynamics and the chemical structure of the wind. We use a simple model to describe the growth of the dust grains under the hypothesis of a time-independent, spherically symmetric stellar wind. Although part of the modelling which describes the stellar outflow is not completely realistic, this approach allows a straight comparison with results based on similar assumptions present in the literature, and thus can be used as an indication of the uncertainties affecting the theoretical investigations focused on the dust formation process in the surroundings of AGB stars.

We find that the total mass of dust injected by AGB stars in the interstellar medium does not increase monotonically with stellar mass and ranges between a minimum of  $10^{-6}M_{\odot}$  for the  $1.5M_{\odot}$  stellar model, up to  $2 \times 10^{-4}M_{\odot}$ , for the  $6M_{\odot}$  case. Dust composition depends on the stellar mass: low-mass stars ( $M < 3M_{\odot}$ ) produce carbon-rich dust, whereas more massive stars, experiencing Hot Bottom Burning, never reach the carbon-star stage, and produce silicates and iron. This is in partial disagreement with previous investigations in the literature, which are based on synthetic AGB models and predict that, when the initial metallicity is  $Z = 0.001$ , C-rich dust is formed at all stellar masses. The differences are due to the different modelling of turbulent convection in the super-adiabaticity regime. Also in this case, like for other physical features of the AGB, the treatment of super-adiabatic convection shows up as the most relevant issue affecting the dust-formation process.

We also investigate Super AGB stars with masses  $6.5M_{\odot} \leq M \leq 8M_{\odot}$  that evolve over a ONe core. Due to a favourable combination of mass loss and Hot Bottom Burning, these stars are predicted to be the most efficient silicate-dust producers, releasing  $[2 - 7] \times 10^{-4}M_{\odot}$  masses of dust.

We discuss the robustness of these predictions and their relevance for the nature and evolution of dust at early cosmic times.

**Key words:** Stars: abundances – Stars: AGB and post-AGB. ISM: abundances, dust

## 1 INTRODUCTION

Winds from stars on the asymptotic giant branch (AGB) and super-asymptotic giant branch (SAGB) provide an important component of mass return into the interstellar medium (ISM) and account for a significant fraction of interstellar dust in present-day mature galaxies (Zhukovska, Gail & Tieloff 2008; Sloan et al. 2009). Recent chemical evo-

lutionary models, which attempt to constrain the origin of the large dust masses inferred from mm and submm data of  $z > 6$  QSOs, have shown that AGB stars give important contributions to the dust content even at these early cosmic epochs (Valiante et al. 2009, 2011).

Observations with the *Spitzer* telescope have probed the formation of dust in AGB stars of galaxies in the Lo-

cal Group (Sloan et al. 2008, 2010a and references therein) and in globular clusters (Sloan et al. 2010b; McDonald et al. 2011). In spite of continuous progress, detailed understanding of the outflow dynamics and grain formation is far from being complete (for a comprehensive review see Höfner 2009): dust grain properties depend on dynamical aspects of the stellar wind, and on the surface chemical composition of the star. Shock waves caused by stellar pulsations lift the gas above the stellar surface intermittently creating dense cool layers where grain condensation can occur. Provided that their cross sections are large enough, the newly formed dust grains can be accelerated by radiation pressure and collisionally couple to the gas, dragging it along. Time-independent wind models, though limited in their capability of reproducing important properties of the dynamical atmosphere with shocks, can reproduce certain observed features, such as the observed spectral energy distribution of C-rich stars with high mass loss rates.

Compared to the problem of computing reliable mass loss rates, the problem of calculating dust yields has the additional complication of estimating the fraction of elements condensing into various types of dust species, which, in turn, depends on the changes in the surface chemistry of the star determined by the interplay between nucleosynthesis and convection.

The most extensive study so far has been made by Ferrarotti & Gail (2006). Using synthetic stellar evolution models, they compute the non-equilibrium dust formation and estimate dust yields for M-, S-, and C-type AGBs. Synthetic AGB models are useful tools, due to the relatively short computation time required and the simplicity with which they can be incorporated in stellar population synthesis studies. On the other hand, they have no predictive power on some key physical processes that occur during AGB evolution, such as the Hot Bottom Burning experienced at the bottom of the convective envelope. A proper description of these processes and of their impact on dust formation demands the full integration of the stellar structure.

To progress in this direction, the aim of the present investigation is to estimate the mass and composition of dust formed around AGBs using models that follow stellar evolution from the pre-main sequence phase. This enables the computation of the time evolution of the surface chemistry and of the mass loss rate in a self-consistent way, providing an important benchmark for studies based on synthetic modelling. Using the proper stellar evolutionary sequences, we also apply the dust formation model to winds of SAGB stars, whose dust yields have not been studied so far.

The paper is organized as follows. The description of the codes used to calculate the AGB and SAGB evolution, the wind structure and dust formation are described in Sect.2; the main physical processes which affect the surface chemistry of these stars are discussed in Sect.3. In Sect.4 we present the resulting dust mass and composition for stars with masses in the range  $1M_{\odot} \leq M \leq 8M_{\odot}$  and with initial metallicity of  $Z = 0.001$ ; we assess the robustness of these results and discuss the effects of uncertain physical processes in Sect.5. Finally, in Sect. 6 we compare our predictions with alternative dust yields present in the literature and in Sect. 7 we summarize the main conclusions.

## 2 PHYSICAL AND NUMERICAL INPUTS

To address the issue of dust production by AGB stars, we developed a specific tool to calculate the structure of the wind around the central object as well as the mass and composition of the newly formed dust. These properties depend on the luminosity, effective temperature and mass loss rate experienced by the star, and on the surface chemical composition. In the following, we provide a description of the numerical code used to integrate the stellar evolution, the ATON code, and of the code used to estimate the stellar wind structure and dust formation.

### 2.1 The ATON evolution code

The evolution of the stars, from their pre Main Sequence phase, until the almost complete ejection of their external mantle, was computed by means of the code ATON (Ventura et al. 1998) which integrates spherically symmetric structures in hydrostatic equilibrium. An exhaustive description of the code is beyond the scope of the present study and we refer the interested reader to the original paper. Here we briefly recall those features which affect the thermodynamics and chemical composition of the wind where dust nucleation occurs.

#### 2.1.1 The convection model

The temperature gradient within regions unstable to convection is determined via the Full Spectrum of Turbulence (Canuto & Mazzitelli (1991), hereinafter FST) model for turbulent convection; the code allows the alternative Mixing Length Theory (MLT) treatment (Vitense 1953). Mixing of chemicals within nuclearly active regions is handled by means of a diffusive approach: for each of the species included in the nuclear network we solve the diffusive equation following the scheme by Cloutman & Eoll (1976), which couples self-consistently nuclear burning and mixing of chemicals. The extra-mixing (overshooting) from the convective borders is simulated by an exponential decay of velocities from the neutrality point, where buoyancy vanishes; the scale of this phenomenon is assumed to be  $l = \zeta H_p$ , where  $H_p$  is the pressure scale height. In agreement with the calibration based on the fit of the observed main sequences of open clusters given in Ventura et al. (1998), we assume  $\zeta = 0.02$  to simulate overshoot from the border of the convective cores during the two major phases of core hydrogen and helium burning. To limit the number of free parameters, we assumed no extra-mixing from the base of the convective envelope during the giant evolution, and during the AGB phase. This choice renders the extent of the Third Dredge Up found during the Thermal Pulses phase a conservative estimate.

#### 2.1.2 The mass loss rate

The mass loss rate during the AGB evolution was modelled according to Blöcker (1995). Based on hydrodynamic computations by Bowen (1988), the strong increase in the mass loss rate during the AGB evolution is modelled by multiplying the Reimers' rate by a given power of the luminosity; the resulting expression is,

$$\dot{M} = 4.83 \times 10^{-22} \eta_R M^{-3.1} L^{3.7} R \quad (1)$$

where  $\eta_R$  is a free parameter and  $M$ ,  $R$ , and  $L$  are the stellar mass, radius and luminosity, expressed in solar units. Using as a calibration the luminosity function of lithium-rich stars in the Magellanic Clouds, we set  $\eta_R = 0.02$  (Ventura et al. 2000).

The Blöcker treatment has been used and tested so far to describe mass loss from high-luminosity, M stars; here we extend this modelling to the C-rich regime, being aware of the additional uncertainties due to this choice on the results obtained. Mattsson et al. (2007) present an analysis of the uncertainties in the description of the mass loss during the AGB phase of carbon stars (see in particular their Fig. 4).

Some sequences based on the Vassiliadis & Wood (1993) treatment (hereinafter VW93) were also calculated for comparison: in this case mass loss increases exponentially with the pulsation period,  $P$ , until the star enters a super-wind phase, when  $P$  exceeds 500d. The super-wind rate is  $\dot{M} = 5 \times 10^{-5} M_\odot/\text{yr}$ .

The results provided by the two descriptions are in reasonable agreement for low-mass AGBs, and for the early AGB phases of the more massive objects; the main differences are found in the description of the advanced phases of the evolution of the stars with mass close to the limit for carbon ignition, where the Blöcker (1995) treatment predicts very large mass loss rates, that favour an earlier consumption of the whole stellar envelope.

### 2.1.3 Nuclear network and opacities

The nuclear network includes 30 elements, with 64 reactions. All the most relevant p-capture and  $\alpha$ -capture processes are taken into account. The nuclear cross-sections were taken from the NACRE compilation (Angulo et al. 1999), with the exception of the reactions  $^{14}\text{N}(p,\gamma)^{15}\text{O}$  (Formicola et al. 2004),  $^{12}\text{C}(\alpha,\gamma)^{16}\text{O}$  (Kunz et al. 2002),  $3\alpha \rightarrow ^{12}\text{C} + \gamma$  (Fynbo et al. 2005),  $^{22}\text{Ne}(p,\gamma)^{23}\text{Na}$  (Hale et al. 2002),  $^{23}\text{Na}(p,\gamma)^{24}\text{Mg}$  (Hale et al. 2004),  $^{23}\text{Na}(p,\alpha)^{20}\text{Ne}$  (Hale et al. 2004).

The opacities in the low-temperature regime are calculated by means of the AESOPUS tool, developed by Marigo & Aringer (2009). These tables are suitably constructed to follow the changes in the chemical composition of the envelope when the C/O ratio approaches, or exceeds, unity. This is deeply different from the classic approach, traditionally used to build AGB models, that neglects possible variations in the surface chemistry during the evolution in the opacity calculations. To understand how the results depend on this choice, we decided to calculate additional AGB models, where the above effect is neglected. It goes without saying that this is expected to play a role only in the models that eventually reach the C-star stage, i.e. for  $M < 4M_\odot$  in the present investigation.

For the present study, we restrict our discussion to stellar models with absolute metallicity  $Z=0.001$ , and helium fraction  $Y=0.24$ . The mixture is  $\alpha$ -enhanced with  $[\alpha/\text{Fe}]=+0.4$ , the solar reference mixture being Grevesse & Sauval (1998). Other chemical compositions will be investigated in future explorations.

## 2.2 Stellar wind and dust formation

The thermodynamic and chemical structure of the wind that forms around AGBs is calculated on the basis of the inputs provided at each time step by the integration of the structure of the central star, which are the natural outcomes of the ATON code. In particular, we use luminosity ( $L$ ), effective temperature ( $T_{\text{eff}}$ ), mass ( $M$ ), mass loss rate ( $\dot{M}$ ), and surface chemistry defined by the mass fractions ( $X_i$ ) of the various elements included in the nuclear network.

### 2.2.1 The structure of the wind

The structure of the wind is determined following the schematization by Ferrarotti & Gail (2006).

The outflow is assumed to be stationary and spherically symmetric. Neglecting the hydrostatic pressure forces, we find from the equation for momentum conservation that,

$$v \frac{dv}{dr} = -\frac{GM}{r^2} (1 - \Gamma). \quad (2)$$

The quantity  $\Gamma$  gives the ratio between the radiative pressure on the dust and the gravitational pull and is given by,

$$\Gamma = \frac{kL}{4\pi cGM}, \quad (3)$$

where  $k$  is the flux-averaged extinction coefficient of the gas-dust mixture and can be expressed as,

$$k = k_{\text{gas}} + \sum_i f_i k_i, \quad (4)$$

with  $k_{\text{gas}} = 10^{-8} \rho^{2/3} T^3$  (Bell & Lin 1994). The sum in eq. (4) is extended to all the dust species considered: the  $f_i$  terms give the degrees of condensation of the key-elements for each dust species and  $k_i$  represent their corresponding extinction coefficients.

To completely define the thermal structure of the wind, we need to specify the density and temperature radial profiles. Mass conservation leads to,

$$\dot{M} = 4\pi r^2 \rho v, \quad (5)$$

and the temperature structure is determined by adopting the approximation by Lucy (1971, 1976) that holds for spherically symmetric, grey winds:

$$T^4 = \frac{1}{2} T_{\text{eff}}^4 \left[ 1 - \sqrt{1 - \frac{R^2}{r^2}} + \frac{3}{2} \tau \right]. \quad (6)$$

The optical depth  $\tau$  in eq. (6) is found from the differential relation,

$$\frac{d\tau}{dr} = -\rho k \frac{R^2}{r^2} \quad (7)$$

with the limiting condition that  $\tau \rightarrow 0$  for  $r \rightarrow \infty$ .

The wind model, determined via integration of eqs. (2)–(7), is calculated starting from the innermost radius where the first dust species become stable, commonly located 3–4 stellar radii away from the centre of the star. This is expected to coincide with the region where  $\Gamma$  increases until

it exceeds unity, and the wind is accelerated to supersonic velocities. In analogy with Ferrarotti & Gail (2006), we keep the velocity of the gas constant from the surface of the star to the region where dust forms. The above equations are integrated out to a radial distance of  $10^4 R$  ( $R$  is the stellar radius), far beyond the point where all the relevant quantities reach their asymptotic behaviour.

Before turning to the dust formation process, we stress here that a more physically sound description of the wind properties is needed before the full reliability of the results from this kind of investigations can be confirmed. In particular, the assumption of a time-independent flow neglects any effect of atmospheric shocks waves, which play a crucial role for the wind mechanism. The assumption of a constant velocity does not account for the consequences of these shocks, which could push the gas beyond the condensation point.

### 2.2.2 Dust formation

Dust formation generally starts with the condensation of small seed nuclei which then grow by accreting material to macroscopic grains. Since the nature of these seeds is still unclear, we do not consider the nucleation phase, but only the growth process of grains. As initial conditions, in agreement with Ferrarotti & Gail (2006), we assume that the seed grains have an initial size  $a_0 = 1\text{nm}$ , and that their initial density is  $n_d = 3 \times 10^{-4} n_H$ , where  $n_H$  is the hydrogen number density in the wind. We could verify that the results are independent of both assumptions.

The composition of dust in the winds during the AGB phase depends on the surface chemical composition. For M stars, with surface  $C/O < 1$ , the dominant dust species are expected to be olivine, pyroxene, quartz, and solid iron. For C stars with surface  $C/O > 1$ , the dust mixture is assumed to be dominated by solid carbon, SiC and solid iron. In Table 1 we summarize the formation reactions of these dust species. When computing the reaction rates for olivine and pyroxene, we follow the variation of the magnesium percentage with respect to the pure iron component.

The temporal variation of the dust grain size for the  $i$ -th dust species,  $a_i$ , is computed as a competition between the growth rate  $J_i^{\text{gr}}$  and the destruction rate  $J_i^{\text{dec}}$ , i.e.

$$da_i/dt = V_{0,i}(J_i^{\text{gr}} - J_i^{\text{dec}}), \quad (8)$$

where  $V_{0,i}$  is the volume of the nominal molecule in the solid. For each dust species, the growth rate is determined by the addition rate of a key element, which is generally the least abundant species involved in the chemical reaction. For silicates and SiC these are supposed to be the SiO and  $C_2H_2$  molecules, respectively, whereas for solid iron and carbon it is the corresponding element in the gas phase. The growth rates per unit time and surface area are proportional to the thermal velocity,  $v_{th}$ , and density,  $n$ , of the key species in the gas phase,

$$J_i^{\text{gr}} = \alpha_i n_i v_{th,i}, \quad (9)$$

where the index  $i$  runs over the different key species and  $\alpha$  is the sticking coefficient.

Vaporization of dust grains by thermal decomposition is estimated from the vapour pressure of the key species,  $p_{v,i}$ , over the solid state, and it is also proportional to the

thermal velocity, reading

$$J_i^{\text{dec}} = \alpha_i v_{th,i} \frac{p_{v,i}}{kT}. \quad (10)$$

For carbon, based on the discussion in Ferrarotti & Gail (2006), we assume that condensation begins at a temperature of 1100 K and that the destruction term is negligible.

The vapour pressures  $p_{v,i}$  in Eq. 10 are found via the law of mass action: it allows to express the individual equilibrium gas pressures of the molecules involved on the basis of the total variation of enthalpy associated to the dust formation reaction. An exhaustive description of the methodology followed to estimate the individual vapour pressures can be found, e.g., in Ferrarotti & Gail (2001).

The formation of the four dust species in M-stars ( $C/O < 1$ ) is therefore characterized by the following four equations,

$$\frac{da_{ol}}{dt} = V_{0,ol}(J_{ol}^{\text{gr}} - J_{ol}^{\text{dec}}), \quad (11)$$

$$\frac{da_{py}}{dt} = V_{0,py}(J_{py}^{\text{gr}} - J_{py}^{\text{dec}}), \quad (12)$$

$$\frac{da_{qu}}{dt} = V_{0,qu}(J_{qu}^{\text{gr}} - J_{qu}^{\text{dec}}), \quad (13)$$

$$\frac{da_{ir}}{dt} = V_{0,ir}(J_{ir}^{\text{gr}} - J_{ir}^{\text{dec}}). \quad (14)$$

These equations are completed by two further relations, giving the percentages of magnesium in the olivine and pyroxene dust particles:

$$\frac{dx_{ol}}{dt} = \frac{3V_{0,ol}}{a_{ol}} \left[ (x_g - x_{ol})J_{ol}^{\text{gr}} + \frac{1}{2}(J_+^{\text{ex}} - J_-^{\text{ex}}) \right] \quad (15)$$

$$\frac{dx_{py}}{dt} = \frac{3V_{0,py}}{a_{py}} \left[ (x_g - x_{py})J_{py}^{\text{gr}} + \frac{1}{2}(J_+^{\text{ex}} - J_-^{\text{ex}}) \right] \quad (16)$$

where  $x_g$  is defined as the relative gas abundance of magnesium with respect to the Mg+Fe sum.

The quantity  $(J_+^{\text{ex}} - J_-^{\text{ex}})$  gives the difference between the exchange rate of iron by magnesium per unit surface area during collisions of Mg with the grain surface and the rate of the reverse reaction, and is given by

$$(J_+^{\text{ex}} - J_-^{\text{ex}}) = v_{th,Mg} \alpha^{\text{ex}} (n_{Mg} - n_{ir} K_p) \quad (17)$$

where  $K_p$  is calculated on the basis of the free enthalpies of formation of the pure products with only magnesium or iron, and  $\alpha^{\text{ex}}$  is the exchange coefficient, describing the probability of exchange of magnesium and iron in the scattering process.

Dust formation in C-stars is described by eq. (14), plus two additional equations for carbon and SiC grains,

$$\frac{da_{SiC}}{dt} = V_{0,SiC}(J_{SiC}^{\text{gr}} - J_{SiC}^{\text{dec}}), \quad (18)$$

$$\frac{da_C}{dt} = V_{0,C} J_C^{\text{gr}}. \quad (19)$$

**Table 1.** Dust species considered in the present analysis, their formation reaction and adopted sticking coefficient (see text).

Grain Species	Formation Reaction	Sticking Coefficient
Olivine	$2x\text{Mg} + 2(1-x)\text{Fe} + \text{SiO} + 3\text{H}_2\text{O} \rightarrow \text{Mg}_{2x}\text{Fe}_{2(1-x)}\text{SiO}_4 + 3\text{H}_2$	0.1
Pyroxene	$x\text{Mg} + (1-x)\text{Fe} + \text{SiO} + 2\text{H}_2\text{O} \rightarrow \text{Mg}_x\text{Fe}_{(1-x)}\text{SiO}_3 + 2\text{H}_2$	0.1
Quartz	$\text{SiO} + \text{H}_2\text{O} \rightarrow \text{SiO}_2(s) + \text{H}_2$	0.1
Silicon Carbide	$2\text{Si} + \text{C}_2\text{H}_2 \rightarrow 2\text{SiC} + \text{H}_2$	1
Carbon	$\text{C} \rightarrow \text{C}(s)$	1
Iron	$\text{Fe} \rightarrow \text{Fe}(s)$	1

The growth rate coefficients  $J_{\text{ol}}^{\text{gr}}$ ,  $J_{\text{py}}^{\text{gr}}$ ,  $J_{\text{qu}}^{\text{gr}}$ ,  $J_{\text{ir}}^{\text{gr}}$ ,  $J_{\text{SiC}}^{\text{gr}}$ ,  $J_{\text{C}}^{\text{gr}}$ , and the exchange coefficients  $J_{+}^{\text{ex}}$ ,  $J_{-}^{\text{ex}}$  for olivine and pyroxene are calculated following Gail & Sedlmayr (1999), Ferrarotti & Gail (2001), Ferrarotti & Gail (2002) and Ferrarotti & Gail (2006). The sticking coefficients for iron, carbon and SiC formation are assumed to be  $\alpha = 1$ , whereas for olivine we take  $\alpha = 0.1$  (see Ferrarotti & Gail (2002), Table 3). For pyroxene and quartz the sticking coefficients are less well determined from laboratory experiments; in analogy with Ferrarotti & Gail (2001), we assume  $\alpha_{\text{py}} = \alpha_{\text{qu}} = 0.1$  (see the last column of Table 1). Finally, the exchange coefficient entering the equation for the determination of the fraction of magnesium within olivine and pyroxene is taken to be  $\alpha^{\text{ex}} = 0.06$ .

The free enthalpy of formation of the molecules involved in the reactions for the condensation of the various species of dust were taken from Sharp & Huebner (1990), with the only exceptions of  $\text{FeSiO}_3$ , graphite, and solid SiC, that were kindly provided by Prof. Gail (private communication).

The extinction coefficients for iron and quartz were calculated according to the analytic expansion given in Gail & Sedlmayr (1999), whereas for olivine and pyroxene we used the opacities derived by Ossenkopf et al. (1992). For what concerns the C-rich environment, we use for SiC eq. (34) in Ferrarotti & Gail (2002), whereas the carbon extinction coefficient was kindly provided by Prof. Gail (private communication). In the cases where analytic expansions associated to solar abundances were used, the coefficients were properly scaled, to account for the difference in the number density of the key-species involved in the present investigation, compared to the solar values.

### 3 THE CHANGE IN THE SURFACE CHEMISTRY OF AGB AND SAGB STARS

After the core He-burning phase is finished, stars with mass  $1M_{\odot} \leq M \leq M_{\text{up}}$  evolve through the AGB phase (see e.g. Herwig (2000)): they experience a series of thermal pulses (TP), triggered by the periodic ignition of a He-rich layer below the CNO burning shell, and end-up as CO White Dwarfs. More massive objects, with  $M_{\text{up}} < M < M_{\text{ccSN}}$ , achieve carbon burning in an off-center, partially degenerate, region; after experiencing some TPs, they evolve as White Dwarfs made up of oxygen and neon. Their evolution is commonly referred to as the Super Asymptotic Giant Branch (SAGB) phase.

The exact values of  $M_{\text{up}}$  and  $M_{\text{ccSN}}$  are determined by the core overshooting during the two major phases of nuclear

burning; in the present investigation, based on the assumption of a moderate extra-mixing from the outer border of the convective core, we find  $M_{\text{up}} = 6M_{\odot}$  and  $M_{\text{ccSN}} = 8M_{\odot}$ .

The mass and composition of dust produced by AGBs and SAGBs is determined both by the physical behaviour of the star and by the surface chemistry. The amount of dust produced will depend on the number density of the key species, which demands a detailed understanding of the evolution of the surface mass fraction of silicon, oxygen, carbon, magnesium and iron.

The surface chemistry of AGBs is affected by two fundamental physical processes, the Third Dredge Up and the Hot Bottom Burning (e.g. Iben & Renzini (1983)). In what follows, we briefly describe the effects of these two mechanisms, and their associated uncertainties.

#### 3.1 Third Dredge Up

The Third Dredge Up (hereafter TDU) is associated to the inwards penetration of the surface convective zone following each thermal pulse (TP), when the bottom of the external mantle crosses the entropy barrier due to the H-He discontinuity; the envelope enters a region where a pulse-driven convective zone, formed as a consequence of the  $3\alpha$  reactions ignition, had spread the products of helium nucleosynthesis; the outcome of such a mechanism is surface carbon enrichment, and the possible achievement of the C-star regime. The TDU modelling is extremely sensitive to the numerics adopted (Straniero et al. 1997): a narrow temporal and spatial zoning, with time-steps of the order of hours, and  $\sim 5000$  mesh-points, are required to allow a self-consistent description of the TDU phenomenology. A deeper TDU can be obtained either by assuming some overshoot from the bottom of the surface convective zone (Herwig 2000), or from the borders of the convective shell that forms when the thermal pulse starts (Herwig & Austin 2004).

For C-rich models, a further source of uncertainty is the adopted low-T radiative opacities. When the C/O ratio approaches unity, the main absorbers of radiation switch from the oxygen bearing molecules, such as  $\text{H}_2\text{O}$ , VO, TiO, to C-bearing molecules, such as CN,  $\text{C}_2$ ,  $\text{C}_3$ ,  $\text{C}_2\text{H}_2$ , which are much more sensitive to the surface mass fractions of the main elements: this makes the C-rich models much more sensitive to the details of the variation of the surface chemical composition of the star. The increase in the absorption of radiation favoured by a larger carbon content is commonly neglected in the computations of the AGB phase, that assume the opacity to depend only on the initial metal content, and disregard any modification of the

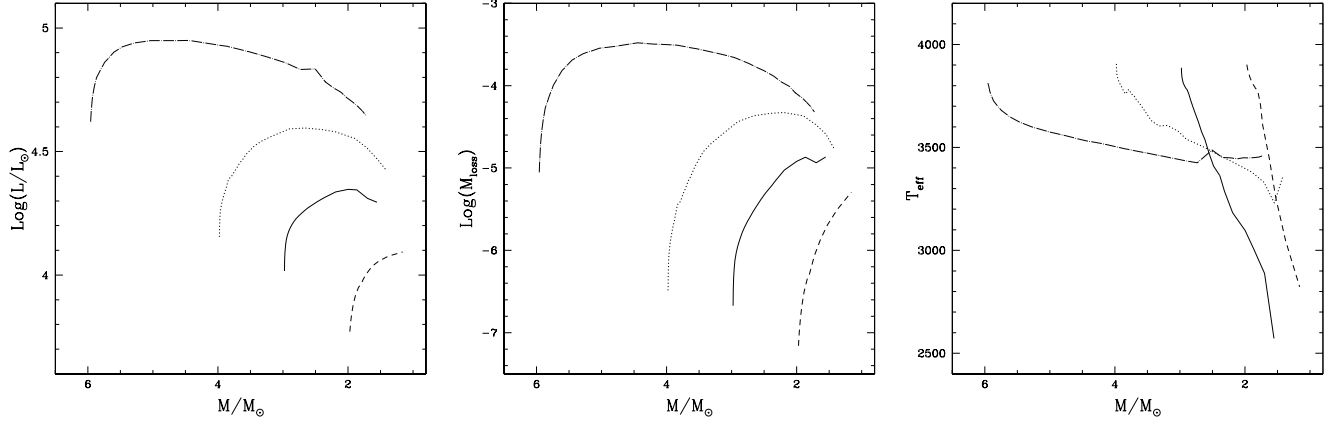


**Figure 1.** The evolution of the luminosity (Left), mass loss rate (Middle, expressed in  $M_{\odot}/\text{yr}$ ) and effective temperature (Right) with the total mass of the star for 4 models with initial mass  $6M_{\odot}$  (dashed-dotted),  $4M_{\odot}$  (dotted),  $3M_{\odot}$  (solid), and  $2M_{\odot}$  (dashed). The low surface temperatures reached by the lower mass models are favoured by the general expansion of the whole convective envelope, that follows the achievement of the C-star stage.

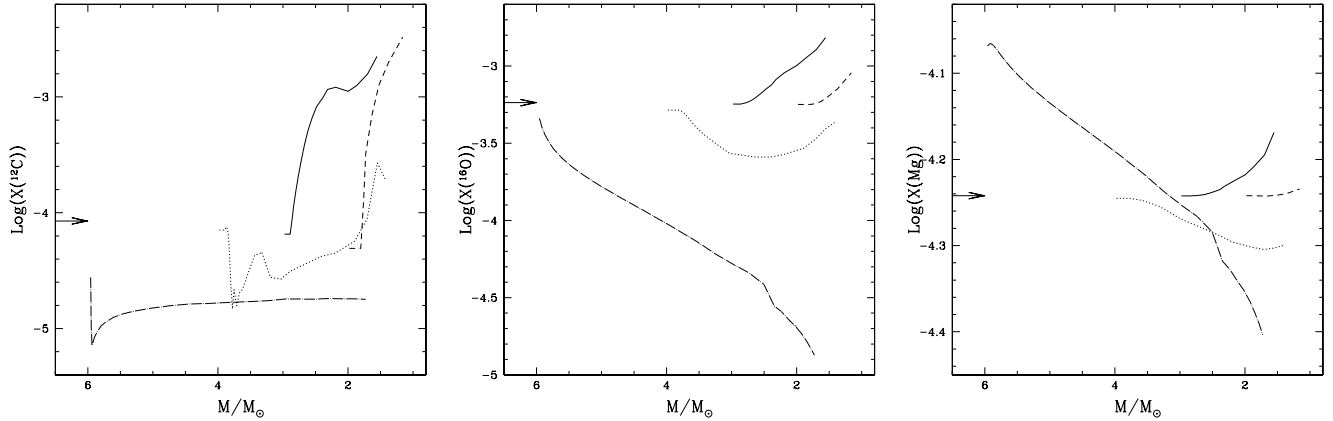


**Figure 2.** The evolution of the surface chemistry of models with different initial masses (same symbols as in Fig. 1) as a function of the stellar mass. The three panels refer to the surface abundances of Carbon (Left), Oxygen (Middle) and total Magnesium (Right). The arrows indicate the initial abundances of the same elements in the original mixture. We note the transition from Hot Bottom Burning, operating in the high-mass regime, and determining a depletion of all the three elements, to the effects of the III Dredge-up, outlined by the increase in the surface carbon mass fraction, dominating in the lowest masses.

surface chemistry. As initially suggested by Marigo (2002), and later confirmed on the basis of full AGB computations (Cristallo et al. 2008; Ventura & Marigo 2009, 2010), the usage of the correct opacities favours a sudden expansion of the structure once C/O reaches unity, which is accompanied by an increase in the mass loss rate experienced; the consumption of the envelope is consequently faster, which prevents the possibility that enormous amounts of carbon are accumulated in the surface regions. An interesting consequence, to be explored also within the context of the present investigation, is that the general cooling of the structure that follows the approach of the C-star stage may potentially quench the Hot Bottom Burning, and favour a C-rich environment.

### 3.2 Hot Bottom Burning

The description of the Hot Bottom Burning (HBB) phenomenology requires a full integration of the whole stellar structure, and a diffusive description of the coupling of nuclear burning and mixing of chemicals within the envelope (Sackmann et al. 1974; Ventura et al. 2000). The HBB phenomenon is a consequence of the delicate coupling between the outer region of the degenerate core, the CNO burning layer, and the innermost regions of the surface convective zone, and by definition cannot be described within the framework of a synthetic modelling of the AGB phase.

Unlike the TDU, HBB conditions are reached during the interpulse phase. The temperature at the base of the external mantle may exceed  $\sim 40 \times 10^6 \text{K}$ , with the consequent activation of p-capture nucleosynthesis. The products of such nuclear activity, due to the rapidity of the convective currents, are immediately transported to the surface. A mild activation of HBB leads to the depletion of carbon,

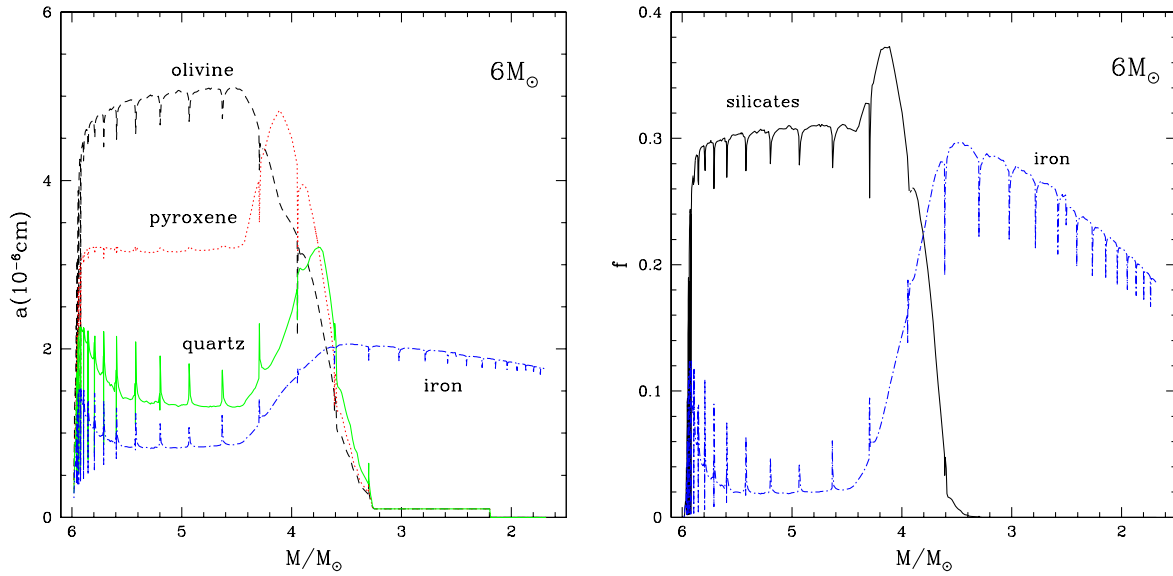


**Figure 3.** Left: Grain size evolution as a function of the total mass of the star during the AGB evolution of a model with initial mass  $6M_{\odot}$ . The different lines correspond to olivine (dashed, black), pyroxene (dotted, red), quartz (solid, green) and iron (dot-dashed, blue). Right: The corresponding evolution of the fraction of silicon condensed into silicate-type dust (solid, black), and of the iron condensed (dot-dashed, blue)

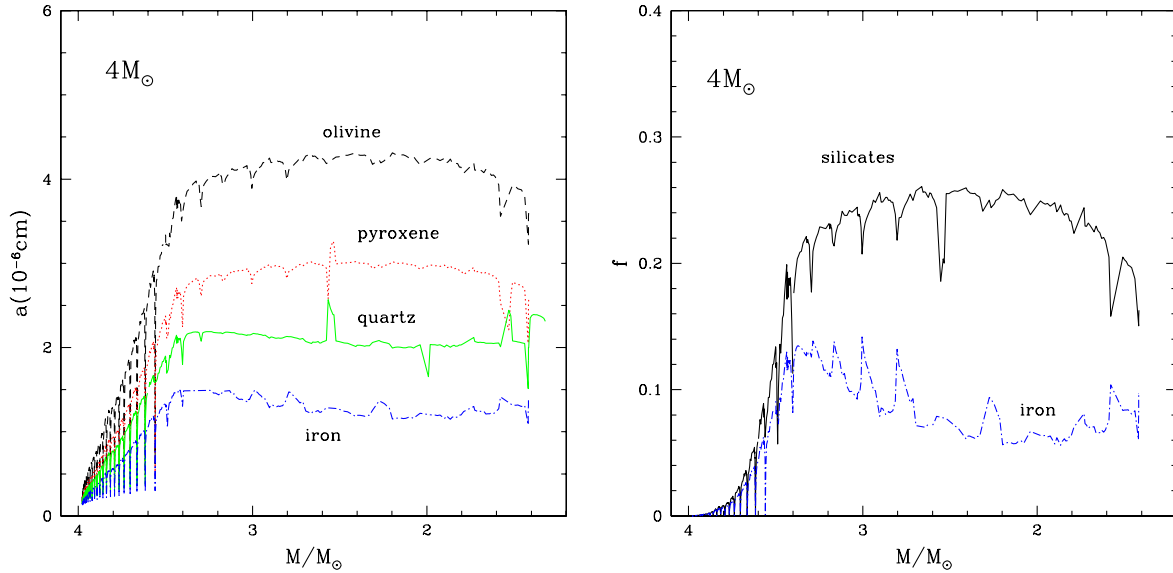


**Figure 4.** Left: The evolution as a function of the total mass of the star during the AGB evolution of the grain size (left) and the fraction of the key elements condensed (right) in a model of initial mass  $4M_{\odot}$ . The meaning of the different lines in the two panels is the same as in Fig. 3.

whereas a stronger HBB may potentially lead to the destruction of the surface oxygen ( $T > 70 \times 10^6$  K); in both cases, a great enhancement of the surface nitrogen is achieved. The modelling of the HBB phenomenology is extremely uncertain, because the thermodynamic stratification of the internal region of the surface convective zone is critically dependent on the convective model adopted: a higher efficiency convective description favours HBB (Renzini & Voli 1981). Blöcker & Schönberner (1991) showed that HBB ignition determines a steep increase in the luminosity of the star, and

a significant deviation from the classic relationship between core mass and luminosity by Paczynski (1970). The major impact of the HBB phenomenology on the AGB evolution was investigated by Ventura & D’Antona (2005a): when convection is modelled following the FST scheme, such as in the reference version of the ATON code, HBB is found in all models for stars more massive than  $\sim 3M_{\odot}$ , and is accompanied by a rapid increase in the mass loss rate experienced by the star, and thus by a faster consumption of the whole

envelope. Only a few thermal pulses are experienced, which prevents the possibility that the C–star stage is reached.

### 3.3 SAGB stars

The main physical properties of massive stars with  $M_{\text{up}} < M < M_{\text{ccSN}}$ , which experience the SAGB phase, have been described in detail by Siess (2006). The recent full exploration by Siess (2010) provides yields that allow to estimate how these stars pollute their surroundings, and to infer the extent of the nucleosynthesis experienced at the bottom of their surface convective zone. The recent investigation by Ventura & D’Antona (2011), via a detailed comparison with the results presented in Siess (2010), showed that: (i) the core masses of this class of objects is so high that HBB conditions are easily achieved, independently of the convection modelling; (ii) the strength of the thermal pulses experienced is modest, thus TDU never occurs, and the C–star stage is never achieved; (iii) the mass loss treatment plays a major role in determining the physical evolution of SAGBs. When a treatment à la Vassiliadis & Wood (1993) is adopted, the star experiences a large number of TPs; the extent of the nucleosynthesis at the bottom of the convective mantle is so high that oxygen is severely depleted (Siess 2010). On the contrary, when the Blöcker (1995) recipe is adopted, the star loses all the envelope before a strong nucleosynthesis may occur.

The SAGB stars are thus expected to experience a strong mass loss since the beginning of their TP evolution, and to show-up traces of p–capture nucleosynthesis, although the rapid consumption of their external mantle prevents the achievement of extended modifications of their surface chemistry.

## 4 WHICH KIND OF DUST FROM AGB AND SAGB STARS?

The quantity of dust formed around a star depends on the gas density in the region where condensation occurs. Within the present schematization, mass conservation imposes a direct relationship between  $\dot{M}$  and  $\rho$  (see Eq. 5): higher densities correspond to large mass loss rates, which renders AGB and SAGB stars particularly suitable for the dust formation process in their surroundings. In the following we describe the results of the model for stars with initial masses in the range  $1M_{\odot} \leq M \leq 8M_{\odot}$  and initial metallicity of  $Z = 0.001$ . The main evolutionary properties of these models were presented and discussed in Ventura & Marigo (2010) and Ventura & D’Antona (2011). Fig. 1 shows the evolution of the main physical properties of four models differing in their initial mass; the three panels refer to the whole AGB phase, during which the stellar envelope is gradually consumed, with a decrease in the stellar mass. The variation of the surface chemistry in the same models is shown in Fig. 2. We limit this description to carbon, oxygen and magnesium, because iron is unchanged, and silicon shows a modest variation ( $\sim +0.05$  dex), and only in the  $6M_{\odot}$  model.

### 4.1 Dust formed under HBB conditions

The left panels of Figs. 3 and 4 show the evolution of dust grain sizes formed in winds of stars with masses  $M = 6M_{\odot}$  and  $M = 4M_{\odot}$  (right panel), that experience HBB. The right panels show the fraction of the key elements condensed into dust: silicon for olivine, pyroxene and quartz, and iron for solid iron. The three panels of Fig. 1 show the evolution of their main physical quantities during the AGB phase (dashed-dotted and dotted lines, for  $6M_{\odot}$  and  $4M_{\odot}$ , respectively), and demonstrate the large luminosities and mass loss rates reached, in particular by the  $M = 6M_{\odot}$  model.

The depletion of the surface carbon (indicated by the initial drop in the carbon mass fraction in the left panel of Fig. 2) prevents the C–star stage to be reached, thus allowing only the formation of silicates and solid iron. Instead of the time coordinate, which increases from left to right, in both Figs. 3 and 4 we show the results as a function of the mass of the star: this helps a better understanding of the amount of dust produced, because the latter depends on the mass lost by the star when the size of the grains is the highest.

Given our choice of convective overshoot from the core during the H–burning phase, the left panel represents the evolution of the largest mass model which evolves through the AGB phase. We can distinguish different phases during the evolution. Dust begins to form as soon as HBB begins, and the mass loss increases. Olivine is the most abundant species and it forms close to the stellar surface; as HBB becomes stronger, the mass loss rate further increases, leading to an increase in the amount of olivine formed but, at the same time, causing a decrease of the least abundant species, i.e. quartz and iron. This result, in agreement with the analysis of Ferrarotti & Gail (2001), is due to the rapid acceleration experienced by the wind as soon as the first species form, which decreases the density of the key species.

The size of the olivine and pyroxene grains decreases at each thermal pulse, as a consequence of the temporary drop in the luminosity (hence of the mass loss rate) of the star. Quartz and iron follow the opposite behaviour, because the smaller mass loss reduces the differences among the amount of dust formed for each species.

We see from Fig. 3 that in the  $6M_{\odot}$  model, when the total mass of the star drops below  $\sim 4M_{\odot}$ , the depletion of surface oxygen (clearly indicated by the slope of the dashed-dotted line in the middle panel of Fig. 2) determines a scarcity of water molecules, required for the formation of the three species of silicates considered (see Table 1). Because the formation of a molecule of olivine requires three  $\text{H}_2\text{O}$  molecules, olivine production stops, followed by pyroxene (which needs only two water molecules), and quartz (one water molecule). From this point on, only iron grains are produced.

We thus find that massive AGB models that experience strong HBB conditions produce a large amount of silicate-type dust during the first part of their AGB evolution, and end-up with iron dust production once the surface abundance of oxygen is strongly reduced. A word of caution concerning this latter possibility is needed here, because the occurrence of an iron-driven outflow might be an artificial effect of the grey description adopted in the present modelling, which favours smaller condensation distances for the iron grains. Simple analytical estimates (Höfner 2009), sup-



ported by detailed models (Woitke 2006), demonstrated that the wavelength dependence of the corresponding grain opacities in the near-IR leads to condensation distances well beyond the reach of shock waves, which means that iron cannot start an outflow, unless the wind is triggered by other types of dust. The possibility of an outflow driven only by iron is thus highly uncertain.

The  $4M_{\odot}$  model (see Fig. 4) evolves at smaller core masses, and can be taken as representative of a star experiencing a milder HBB. Compared to the  $6M_{\odot}$  case, due to the smaller  $\dot{M}$ , less silicates are produced in the early AGB phases; on the other hand, the depletion of oxygen is less severe (see middle panel of Fig. 2), thus silicates continue to form throughout the AGB evolution. These two effects compensate each other, thus the two models, at the end of the evolution, produce approximately the same quantity of silicates and a total dust mass of  $\sim (1.2 - 2) \times 10^{-4} M_{\odot}$  (see Table 2). The lower mass loss also leads to smaller differences among the various types of dust formed.

## 4.2 Dust from C-rich environments

Models whose initial mass is below  $3.5M_{\odot}$  hardly reach HBB conditions, and evolve at smaller luminosities compared to their more massive counterparts (see the left panel of Fig. 1). The repeated TDU episodes eventually leads to the formation of a C-star, as indicated by the great increase in the surface carbon content for the models with initial mass  $2M_{\odot}$  and  $3M_{\odot}$  shown in the left panel of Fig. 2. This is accompanied by a switch from silicate-type dust to C-rich particles. In the left panels of Figs. 5 and 6 we show the grain size evolution as a function of the mass of the star for two models with  $3M_{\odot}$  and  $2M_{\odot}$ ; the right panels show the degree of condensation of the key elements (essentially, carbon and silicon in this case). In both cases we note an initial modest production of silicates, that proceeds until C/O reaches unity. From that point on, solid carbon and SiC are formed. The decrement in the dimension of carbon grains during each interpulse period in the  $3M_{\odot}$  model is an effect of HBB, which is completely absent in the  $2M_{\odot}$  model. In this latter case, representative of all the models that show no effects of HBB, a large amount of carbon grains are expected to form around the star. Unlike their more massive counterparts, low-mass AGBs progressively increase their surface carbon content due to the repeated TDUs, and produce more and more dust as they evolve, until no mass is left within the convective envelope. The total mass of dust formed by stars with  $M \leq 3.5M_{\odot}$  ranges between  $\sim (0.01 - 7.7) \times 10^{-4} M_{\odot}$  (see Table 2).

## 4.3 Dust from SAGB stars

SAGB stars evolve at large luminosities since the first TPs, and experience a strong mass loss rate that favours an early consumption of their convective envelope. Fig. 7 shows the variation of the overall fraction of silicon condensed into silicate-type dust as a function of the total stellar mass. The different lines correspond to SAGB models with masses in the range  $6.5M_{\odot} \leq M \leq 8M_{\odot}$  published in Ventura & D'Antona (2011). For comparison, the most massive AGB model ( $6M_{\odot}$ ) previously discussed is also shown.

It is evident that the mass of silicate dust grains produced by SAGBs is larger than in the  $6M_{\odot}$  model, for two main reasons: (i) since SAGBs evolve at large core masses, their luminosity and mass loss are extraordinarily large since the very first TPs and (ii) unlike the most massive AGBs, oxygen is not depleted extensively, because the envelope is lost before the nucleosynthesis experienced at the bottom of their surface mantle can reach very advanced stages. Thus, silicates continue to form during the whole TPs evolution because water molecules are always available in their surroundings. The total masses of dust formed by SAGBs vary in the range  $\sim (3 - 7) \times 10^{-4} M_{\odot}$  (see Table 2).

## 4.4 Stardust from AGB and SAGB stars

In Table 2 we list the total dust masses and the masses of individual dust species predicted by the model for the investigated grid of stellar masses. Similarly to other important AGB phenomena, the key quantity which determines the composition of dust formed around the star is the core mass,  $M_{\text{core}}$ : models with small  $M_{\text{core}}$  achieve only a modest production of silicates, whereas carbon is produced in great quantities. In the more massive objects the opposite situation occurs, since HBB prevents the formation of any carbon-rich dust species, whereas a strong production of silicates is favoured.

Fig. 8 shows the total mass of dust as a function of the initial stellar mass (solid line) and the contribution of individual dust species (i.e. silicates, iron, carbon, and SiC). The results refer to AGB and SAGB models calculated with the reference ATON model discussed in Sect. 4.

We note a doubled-peaked distribution, with a maximum production of carbon by low-mass AGBs and of silicates by SAGBs; stars with  $3M_{\odot} < M < 5M_{\odot}$  provide the smallest contribution to dust formation, because the production of carbon is inhibited by HBB, which is however too soft to allow a large silicates production. At stellar masses around  $\sim 3M_{\odot}$  (this result depends on the treatment of the low-T molecular opacities, see Sec. 5.1) we note the transition from carbon-rich to silicate-rich dust, which is a pure effect of HBB, prevailing over the TDU effects.

The mass of silicates formed by stars in the mass range  $[4 - 6]M_{\odot}$  is approximately constant: this is a consequence of the strong production of silicates, achieved in the early AGB phases in the more massive models, counterbalanced by the scarcity of the water molecules available for the condensation process, due to the very strong and fast depletion of oxygen, that characterize the latest evolutionary stages. The SAGB models, are, under the present assumptions, the most efficient silicates producers, for the reasons discussed in Sect. 4.3.

## 5 DEPENDENCE OF DUST PRODUCTION ON PHYSICAL PARAMETERS

In the previous section we have presented the results of the dust formation model for different stellar masses. Here we discuss how uncertainties in the modelling of the AGB/SAGB evolution and in the physics of dust formation may affect the robustness of these findings. In particular,

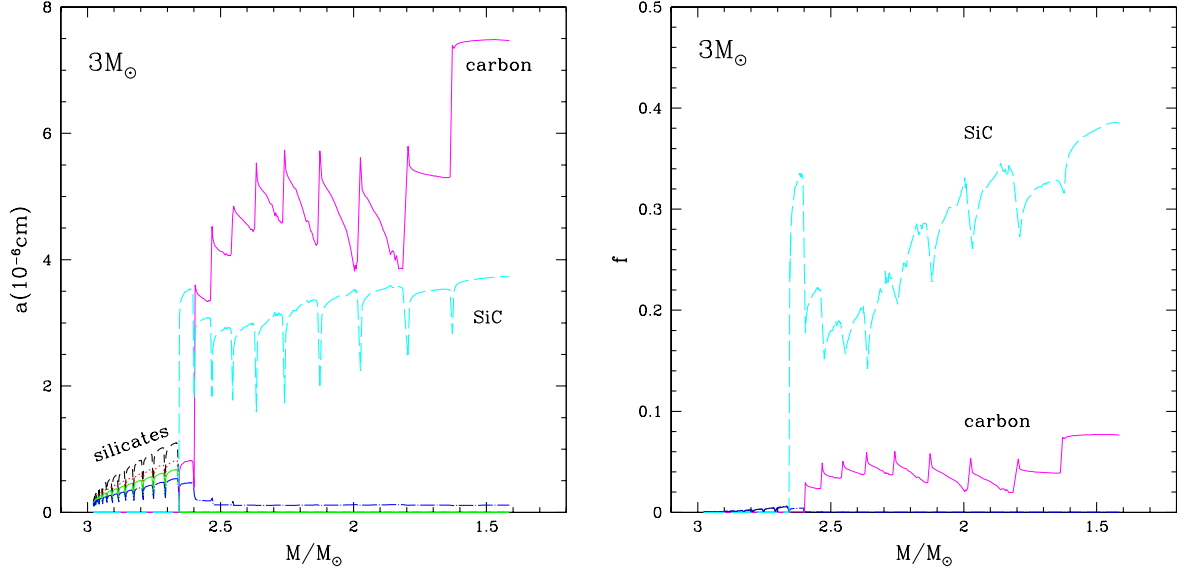


**Figure 5.** The same as Fig. 3, but for a stellar model with initial mass  $3M_{\odot}$ . Line coding for silicates and iron (whose production is however negligible in the present model) is the same as in Fig. 3. Light solid, magenta lines indicate the evolution of carbon grain size (left panel) and of the fraction of carbon condensed (right); Long-dashed, cyan lines show the variation of the SiC grain size (left) and of the fraction of silicon condensed into SiC (right). We note the effects of the transition from M stars to C stars, when no silicates are produced.

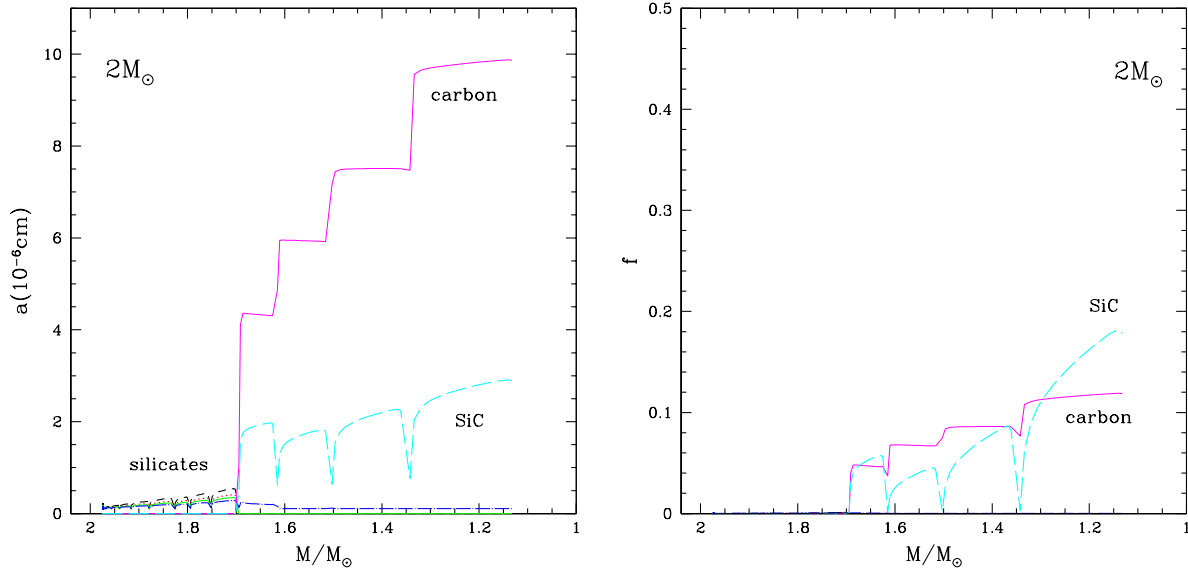


**Figure 6.** The same as Fig. 5, but for a stellar model with initial  $2M_{\odot}$  (right).

we examine the role played by the adopted low- $T$  molecular opacities, the mass loss treatment, and the chosen set of sticking coefficients. A discussion of the impact of the adopted convective model is presented in Sect. 6.

### 5.1 Low- $T$ molecular opacities

The models presented and discussed so far (see, in particular, Figs. 5 and 6) are based on a modern and updated method to determine the molecular opacities in the low

temperature regime: the AESOPUS tool (Marigo & Aringer 2009), that accounts for the changes in the chemistry of the envelope to calculate the absorption coefficient,  $k$ , in the most external regions of the star.

In the traditional approach, the evolution of the surface abundances of the various species is ignored: the opacity is determined on the basis of the initial composition of the star, neglecting the increase in the surface carbon abundance provided by TDU.

Since previous studies of dust production by AGBs rely on this latter approximation, we have quantified the differ-

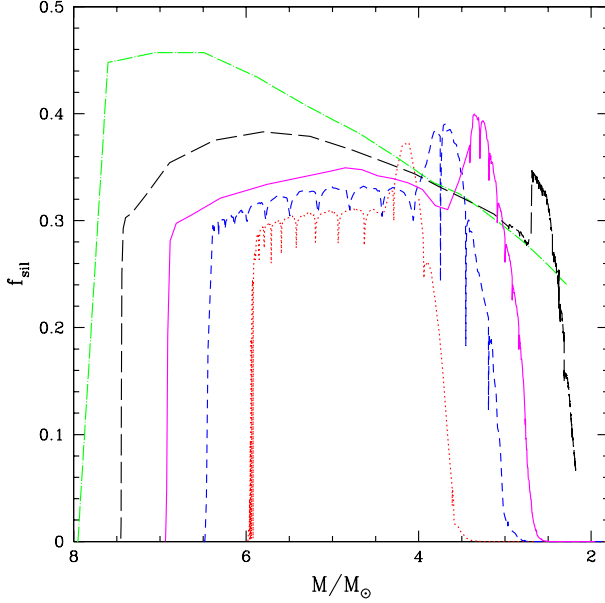


**Figure 7.** The total fraction of silicon condensed into silicate dust grains as a function of the total stellar mass in SAGB models with initial masses of 6.5 (dashed, blue), 7 (solid, magenta), 7.5 (long-dashed, black), and 8  $M_{\odot}$  (dot-dashed, green). For comparison, we also show the results obtained for the most massive AGB model with  $M = 6M_{\odot}$  (dotted, red line).

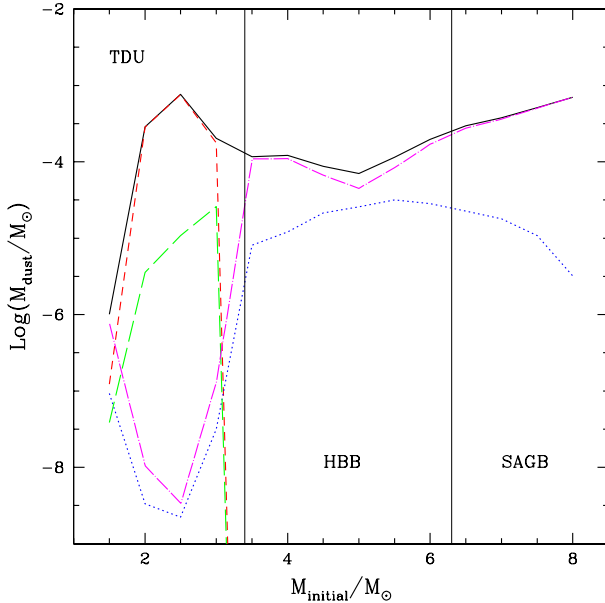


**Figure 8.** The total mass of dust produced by AGB & SAGB models of different masses (solid, black line). We also show the total mass of the individual components, indicated as follows: Silicates (dot-dashed, magenta), carbon (dashed, red), SiC (long-dashed, green), iron (dotted, blue).

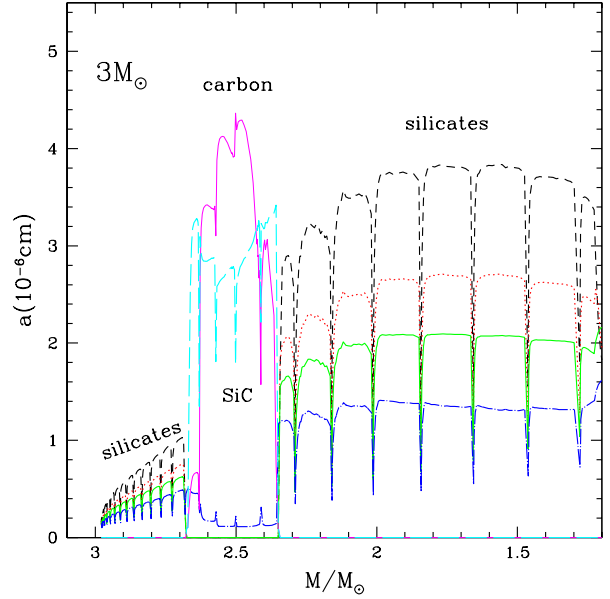


**Figure 9.** The dust produced by a  $3M_{\odot}$  model in which, as in previous works, the increase in the surface carbon is neglected in the computation of the low-T opacities. The dimensions of the different types of dust produced are indicated with the same symbols as in Fig. ???. The comparison with the results shown in the left panel of Fig. ?? allows us to understand the role played by the low-T opacity description: we note that in this case HBB is not extinguished, thus the production of carbon-rich dust is limited to a narrow time-interval, before strong HBB destroys the surface carbon available.

ences introduced by the new method to calculate the opacities in terms of the total mass of dust formed. We thus calculate a further set of AGB models in which the traditional method was used to compute  $k$  in the low-T regime.

As long as the C/O ratio is  $< 1$ , such as in the most massive AGB models which experience HBB, the evolution is independent of the opacity treatment (Ventura & Marigo 2010). We thus restrict our analysis to lower mass stars ( $M \leq 3M_{\odot}$ ), whose surface chemistry is dominated by TDU.

Fig. 9 shows the resulting grain size evolution for a  $3M_{\odot}$  star; this is to be compared with the left panel of Fig. 5, that refers to a model with the same mass, calculated with the AESOPUS tool. Both models achieve an early small production of silicate-type dust, that proceeds until repeated TDU episodes allow to reach the C-star stage. From this point on, the predictions diverge. When the opacities are computed with the AESOPUS tool, carbon-rich dust continues to be produced during the whole AGB phase. On the other hand (see Fig. 9), when the traditional opacities are used, C and SiC grains are produced only within a narrow range of stellar mass, after which silicates production takes over again. This is a consequence of the quenching of HBB, that was early predicted by Marigo (2002), and later confirmed by Ventura & Marigo (2009): because the core mass of a  $3M_{\odot}$  star is the minimum allowing HBB conditions, the expansion of the envelope following the increase in the surface carbon is sufficient to turn off HBB: this is favoured by the rapid increase of AESOPUS opacities that accompanies the achievement of the C-star stage. The model shown in

Fig. 9 does not follow this behaviour due to the use of classical opacities; the star eventually reaches HBB conditions and silicates production takes over again.

The  $3M_{\odot}$  model just discussed lies within the narrow range of masses ( $\delta M \sim 0.5M_{\odot}$ ) where the differences caused by the two opacity treatments are most dramatic, affecting both the resulting grain composition and the total mass of dust produced: when the traditional opacities are adopted, the total mass of dust produced is  $7 \times 10^{-5}M_{\odot}$  (to be compared with the corresponding value in Tab. 2, i.e.  $\sim 2 \times 10^{-4}M_{\odot}$ ), most of which is silicate-type dust. Stars with  $M \leq 2.5M_{\odot}$  do not experience any HBB and the low-T opacity treatment affects only the total mass of C-rich dust formed, which is approximately a factor  $\sim 2$  smaller when the AESOPUS tool is used. In fact, the increase in the surface carbon abundance is accompanied by a general expansion of the whole structure, and by a faster consumption of the whole envelope, resulting in a smaller surface carbon content.

It is important to remark that the above conclusions depend on the adopted mass loss rate. As shown by Ventura & Marigo (2010), the physical and chemical evolution of low-mass AGB stars depend on the interplay between mass loss rate and molecular opacities: a smaller  $\dot{M}$  favours HBB and thus shifts downwards the range of masses dominated by TDU, around which the formation of carbon-type dust occurs.

## 5.2 The mass loss treatment

The mass loss description has important effects on dust formation around AGBs. In fact, the surface chemistry of the star, which determines the composition of dust species, results from the interplay among TDU, HBB, and the consumption rate of the envelope. This is particularly important for massive AGBs and SAGBs, because the degree of the p-capture nucleosynthesis experienced at the base of the convective zone, hence the final elemental abundances, depends on the mass left in the envelope at each evolutionary stage. Therefore, a major issue is the competition between the rates of the relevant nuclear reactions and the time-scale for envelope consumption. In the reference ATON model, the mass loss treatment follows the prescription by Blöcker (1995). To quantify the uncertainties introduced by the mass loss treatment we have explored models where the Vassiliadis & Wood (1993) prescription is used.

The evolution of the  $6M_{\odot}$  model presented in Fig. 3 is characterized by an early phase of strong silicates production, followed by a later stage, during which only solid iron forms. When silicates production ceases, the mass left on the envelope depends on the ratio between the rate of oxygen burning at the bottom of the external mantle and the rate of envelope ejection: a smaller  $\dot{M}$  renders this behaviour even more extreme, because it increases the fraction of silicates-free mass lost by the star. This is illustrated in Fig. 10. The left panel shows the variations of the surface content of oxygen and carbon when the Blöcker (1995) (solid lines) and the Vassiliadis & Wood (1993) (dotted lines) mass loss treatments are used. In both models, an initial phase of carbon burning occurs, followed by the depletion of surface oxygen. The Blöcker (1995) mass loss is so strong that oxygen burning proceeds at the same rate as surface man-

tle consumption. Since the Vassiliadis & Wood (1993) mass loss rate is much slower, the star experiences many more TPs, and eventually TDU, via an increase in the surface  $^{12}\text{C}$ , favours the formation of a carbon star. However, carbon dust production is negligible because surface carbon enrichment is inhibited by HBB. For the  $6M_{\odot}$  stellar mass model, the mass lost by the star when it is still O-rich is  $\Delta M \sim 1M_{\odot}$ , to be compared to  $\Delta M \sim 3M_{\odot}$  in the Blöcker (1995) model. As it is shown in the right panel of Fig. 10, the production of silicates is consequently smaller and iron is the only dust species produced for most of the evolution. As a result, the lower mass loss rate leads to a reduction of the total dust mass produced by  $\sim 2$  dex.

Dust formation is progressively less affected by the mass loss description as the mass of the star decreases, because stars of smaller mass never enter the phase when only iron is produced, thus the production of silicates never ceases.

As discussed in Sect. 5.1, mass loss also plays a role in setting the stellar mass, which marks the border between silicates producers and carbon-dust producers. With our standard choices, based on the Blöcker (1995) treatment, we find this threshold mass to be  $M \sim 3M_{\odot}$ . When the Vassiliadis & Wood (1993) formulation is adopted, this limit shifts downwards to  $M \sim 2.5M_{\odot}$ , because the larger mass left in the envelope for a given core mass favours HBB ignition.

For SAGBs, Ventura & D’Antona (2011) showed that a mass loss rate increasing with the luminosity, as in the Blöcker (1995) recipe, prevents the star from experiencing a very advanced nucleosynthesis; on the contrary, in models based on the Vassiliadis & Wood (1993) formulation only a modest amount of oxygen is left in the envelope for most of the SAGB evolution (Siess 2010). In this latter case the production of silicates would be smaller and limited to early evolutionary phases, whereas iron would be the main dust species produced. A detailed investigation, aimed at understanding the uncertainties affecting stardust from SAGB stars, is in preparation and will be presented in a separate paper.

## 5.3 The sticking coefficients

For each dust species, condensation occurs below a threshold temperature that depends on the differences in the formation enthalpies of the various molecules entering the reaction associated to the condensation process. Below the threshold temperature, the destruction rate rapidly declines to zero, thus leaving the production rate to depend uniquely on the growth-rate coefficients. The latter, in turn, are linearly proportional to the sticking coefficients,  $\alpha$ , which parametrize the efficiency of the dust formation process.

For quartz and pyroxene the sticking coefficients are poorly constrained by laboratory experiments. Similarly, the exchange coefficient regulating the magnesium fraction within olivine and pyroxene is very uncertain. Since for all the stellar models the surface chemical composition is extremely rich in magnesium, the latter coefficient has a negligible effect on dust formation and the equilibria of both hybrid products, olivine and pyroxene, are always shifted to the magnesium-rich cases.

To estimate the uncertainties associated to the sticking coefficients we have artificially changed by a factor 5 those

**Table 2.** Dust mass produced by AGB and SAGB models, assuming an initial metallicity  $Z = 0.001$ . The initial stellar mass  $M$  and the core mass  $M_{\text{core}}$  are reported in the first and second columns. The total mass of dust,  $M_d$  and the mass of pyroxene ( $M_{\text{py}}$ ), quartz ( $M_{\text{qu}}$ ), solid iron ( $M_{\text{ir}}$ ), solid carbon ( $M_C$ ) and SiC ( $M_{\text{SiC}}$ ) are also shown. All the masses are expressed in solar units.

$M$	$M_{\text{core}}$	$M_d$	$M_{\text{ol}}$	$M_{\text{py}}$	$M_{\text{qu}}$	$M_{\text{ir}}$	$M_C$	$M_{\text{SiC}}$
1.5	0.530	1.01d-06	4.97d-07	1.89d-07	6.97d-08	9.25d-08	1.23d-07	3.85d-08
2.0	0.533	2.88d-04	6.19d-09	2.88d-09	1.30d-09	3.34d-09	2.84d-04	3.55d-06
2.5	0.645	7.67d-04	1.97d-09	9.68d-10	4.52d-10	2.23d-09	7.56d-04	1.08d-05
3.0	0.711	2.03d-04	8.50d-08	3.50d-08	1.43d-08	3.17d-08	1.77d-04	2.60d-05
3.5	0.812	1.17d-04	7.40d-05	2.63d-05	8.19d-06	8.12d-06	-	-
4.0	0.842	1.21d-04	7.22d-05	2.70d-05	9.56d-06	1.21d-05	-	-
4.5	0.877	8.76d-05	3.55d-05	2.12d-05	9.59d-06	2.13d-05	-	-
5.0	0.914	7.05d-05	2.66d-05	1.31d-05	4.97d-06	2.58d-05	-	-
5.5	0.959	1.15d-04	5.18d-05	2.53d-05	5.93d-06	3.16d-05	-	-
6.0	1.012	1.96d-04	1.11d-04	5.04d-05	6.64d-06	2.84d-05	-	-
6.5	1.086	2.97d-04	1.94d-04	7.29d-05	7.63d-06	2.26d-05	-	-
7.0	1.260	3.77d-04	2.74d-04	7.81d-05	7.09d-06	1.79d-05	-	-
7.5	1.308	5.11d-04	4.14d-04	7.33d-05	1.33d-05	1.08d-05	-	-
8.0	1.348	6.98d-04	6.11d-04	8.02d-05	4.12d-06	3.21d-06	-	-

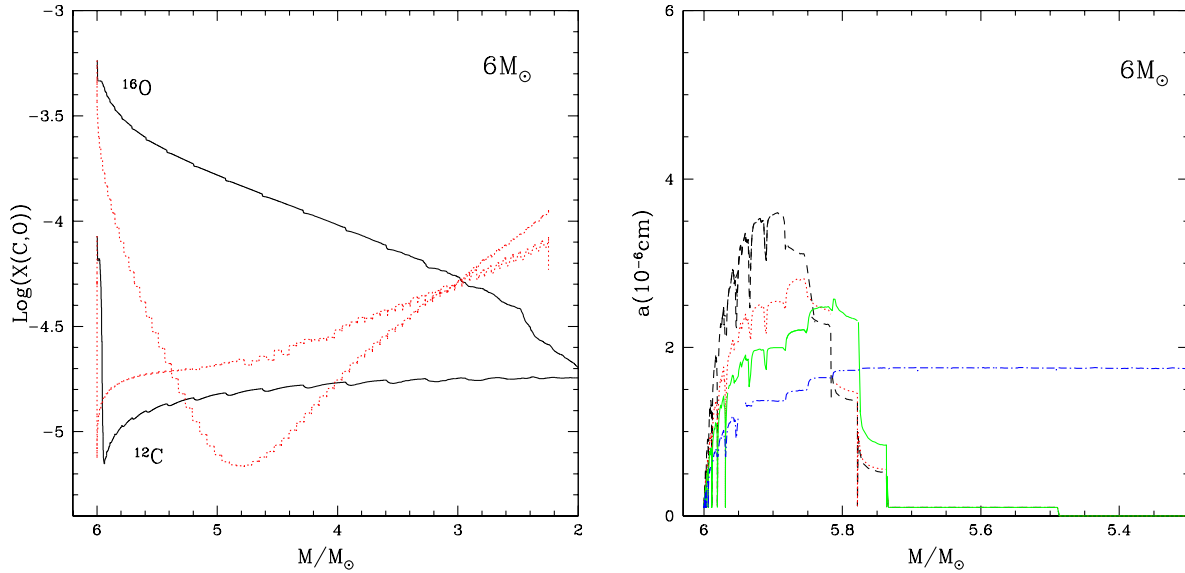


**Figure 10.** Left: the variation of the surface content of oxygen and carbon in two models of mass  $6M_{\odot}$  in which the mass loss was modelled according to the prescriptions by Blöcker (1995) (solid, black line) and Vassiliadis & Wood (1993) (dotted, red). In this latter case only a little fraction of the stellar mass is lost by the time that the surface oxygen almost disappears, thus the star enters the C-star regime, and the silicates production stops. The right panel (to be compared to the left panel of Fig. ??, that shows the corresponding evolution calculated with the Blöcker (1995) recipe for mass loss) shows that the silicates production is extremely poor, and the star produces iron for the almost totality of its evolution. Note that the small carbon abundances inhibit the formation of C-rich dust particles, even in conditions of  $C/O > 1$ .

relative to pyroxene and quartz (see Table 1 for the values adopted in the reference model). The resulting dust masses are shown in Fig. 11 where dashed (solid) lines indicate the mass of pyroxene (quartz) expected when the minimum and maximum sticking coefficient is adopted. For comparison, we also show the total mass of silicates expected in the reference model (filled squares) and mass of olivine (long-dashed line) which is not affected by the uncertainty on the sticking coefficient and is the most abundant species among silicates. Thus, although the pyroxene and quartz masses can vary by a factor  $\sim 20$ , their variation has a smaller effect on the total mass of dust: this is represented by the shaded

region and shows that when the lowest limits for the pyroxene and quartz sticking coefficients are used, their contribution is completely negligible compared to the olivine, causing a  $\sim 30\%$  decrease in the total mass of silicates. On the other hand, with the highest sticking coefficient, pyroxene becomes the dominant species for all stellar models, and the silicates mass produced increases by a factor  $\sim 3$ . At present, this quantifies the degree of uncertainty due to choice of the sticking coefficients on the total dust mass formed.

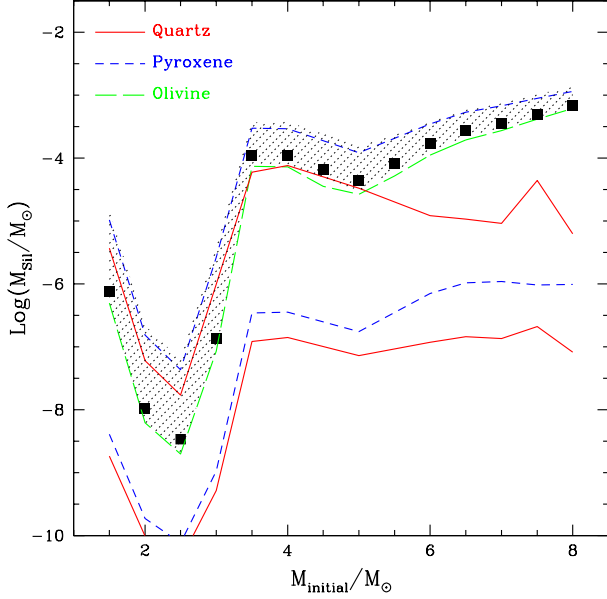


**Figure 11.** The filled squares indicate the total mass of silicates estimated by the reference model as a function of the initial stellar mass with the shaded region illustrating the uncertainty induced by variations of pyroxene and quartz sticking coefficients. The dashed (blue) and solid (red) lines indicate, respectively, the lowest/highest masses of pyroxene and quartz produced when the corresponding sticking coefficients are decreased/increased by a factor 5 with respect to the reference values shown in Table 1. The long-dashed line indicates the mass of the olivine-type dust produced in the reference model.

## 6 DISCUSSION

In Fig. 12 we summarize the results of the present study of dust production by AGBs and SAGBs stars. We show separately the silicates (left panel) and carbon (right) dust produced by stars as a function of their initial mass. The values obtained with the reference model for the AGB evolution described in Sect. 2 are indicated as filled squares. The shaded areas quantify the uncertainties introduced in dust mass estimates by the poorly understood physical processes discussed in the previous sections. These are limited to stellar masses  $M \leq 6M_{\odot}$  because a detailed investigation of the uncertainties affecting dust production by SAGBs will be presented in a future paper. For comparison, the triangles represent the results obtained by Ferrarotti & Gail (2006) using synthetic models of AGBs with initial metallicity of  $Z = 0.001$ .

The extension of the shaded region in the left panel of Fig. 12 confirms that the mass of silicates produced by stars with  $M \leq 3M_{\odot}$  is extremely uncertain, being very sensitive to the adopted molecular opacities whose treatment determines whether HBB can be activated. In our standard case, models within this range of masses are predicted to produce carbon-type dust, with a poor production of silicates: this explains the almost null lower limit in the left panel of Fig. 12. On the other hand, use of classic opacities, coupled with the Vassiliadis & Wood (1993) mass loss prescription, allows HBB conditions to be reached even for  $M \sim 2M_{\odot}$ , thus preventing the envelope of the star to become carbon-

rich, and favouring the production of silicate-type dust. These assumptions, coupled with the highest choice of the sticking coefficients for the formation of pyroxene and quartz grains (see Fig. 11), determine the upper envelope of the shaded area in the low-mass regime of Fig. 12 (left panel).

For stars experiencing HBB, the uncertainties on silicates production are smaller. The lower limit on the shaded regions is set by the mass loss modelling, whereas the upper limit is due to the choice of the sticking coefficients. In agreement with the discussion of the previous sections, we find that the most uncertain models are those experiencing strong HBB ( $M \sim 6M_{\odot}$ ).

The right panel of Fig. 12 shows that carbon dust production is also uncertain in the low-mass regime ( $M \leq 3M_{\odot}$ ), due to the combined effects of mass loss and opacities for carbon-rich mixtures, that are essential in determining whether HBB conditions are reached. In our reference model no carbon dust is expected for  $M > 3.5M_{\odot}$ , whereas in models calculated with the Vassiliadis & Wood (1993) mass loss treatment some production is expected, because the envelope is consumed so slowly that eventually TDU can lead to the  $C/O > 1$  condition. This determines the extent of the shaded region associated to stars of  $4M_{\odot}$  in the right panel of Fig. 12.

A comparison between the data marked with squares and triangles in Fig. 12 shows that the dust yields based on synthetic AGB models (Ferrarotti & Gail 2006) can not be reconciled with our results, even taking into account the uncertainties on the physical processes discussed so far. According to Ferrarotti & Gail (2006), the dominant dust species produced by stars with  $Z = 0.001$  and initial stellar masses  $1M_{\odot} \leq M \leq 7M_{\odot}$  is carbon-dust; the production of silicates is limited to stars with initial masses  $\geq 4M_{\odot}$  but amounts to a few percent of the total dust mass formed.

These differences can be entirely ascribed to the adopted description of the convective transport in the innermost regions of the convective envelope. As shown by Ventura & D’Antona (2005a), use of the FST model leads to stronger HBB, at odds with the MLT treatment, that favours a modest HBB only in the most massive stars. In the latter case, independently of the mass, TDU eventually dominates and the carbon-star stage is reached. It is not surprising that the results by Ferrarotti & Gail (2006) predict the formation of C-type dust; in our case this is possible only for models not experiencing HBB, i.e. for  $M \leq 3M_{\odot}$ .

In the low-mass regime the results are in qualitative agreement, the carbon-dust mass presented by Ferrarotti & Gail (2006) being larger; this is partly due to the different choices for the low-T molecular opacities and the mass loss description, and also the efficiency of the TDU extension, which in our case is found by neglecting any overshoot from the base of the envelope, and is thus to be considered as a conservative estimate.

### 6.1 Implications for cosmic dust enrichment

It is interesting to investigate the implications of the dust yields for AGB and SAGB stars within the context of cosmic dust enrichment.

Following the analysis done by Valiante et al. (2009), we can estimate the time evolution of the dust mass (and of individual dust species) produced by a stellar population

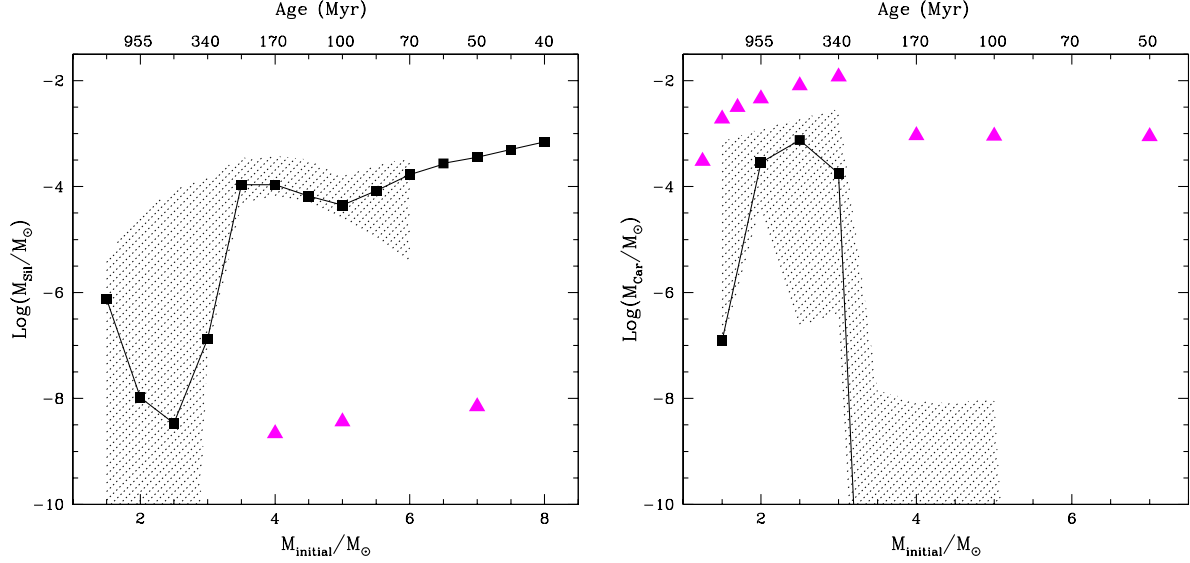


**Figure 12.** The mass of silicates (left) and carbon dust (right) formed around AGB and SAGB models of a given initial mass. Data points represented by filled squares indicate the results of our reference AGB and SAGB models. The shaded areas in both panels illustrate the overall uncertainties associated to these predictions (see text). For comparison, the dust yields predicted by Ferrarotti & Gail (2006) are also shown (filled triangles). Times on the upper axis indicate for each initial mass the duration of the evolutionary phases preceding the beginning of AGB.

as,

$$M_{\text{dust}}(t) = \int_0^t dt' \int_{m_*(t')}^{m_{\text{up}}} m_{\text{dust}}(m) \phi(m) SFR(t' - \tau_m) dm, \quad (20)$$

where  $m_{\text{dust}}(m)$  are the stellar mass dependent dust yields,  $\phi(m)$  is the stellar initial mass function (IMF),  $m_{\text{up}}$  is the upper limit of the stellar mass range,  $\tau_m$  is the lifetime of a star with mass  $m$ ,  $SFR$  is the star formation rate and  $m_*(t')$  is the mass of a star with lifetime  $\tau_{m_*} = t'$ . We adopt a Larson IMF (Larson 1998) which follows a Salpeter-like power-law at the high-mass end but flattens below a characteristic stellar mass,  $m_{\text{ch}} = 0.35 M_{\odot}$ ,

$$\phi(m) \propto m^{-(\alpha+1)} e^{-m_{\text{ch}}/m}, \quad (21)$$

where  $\alpha = 1.35$  and the IMF is normalized between  $m_{\text{inf}} = 0.1 M_{\odot}$  and  $m_{\text{up}} = 100 M_{\odot}$ . For stars with masses in the range  $1 M_{\odot} \leq m \leq 8 M_{\odot}$ , we take the AGBs and SAGBs dust yields predicted by the reference model discussed in Sec. 4. At larger stellar masses, dust can be synthesized in the ejecta of core-collapse SNe and dust yields as a function of the progenitor mass and metallicities have been published in the literature (Kozasa, Hasegawa & Nomoto 1991; Todini & Ferrara 2001; Nozawa et al. 2003; Bianchi & Schneider 2007). Here we neglect this contribution to dust production and we only consider the AGBs and SAGBs dust yields.

The time evolution of the total dust mass, described by eq. 20, depends also on the stellar lifetimes and on the adopted star formation history. For low and intermediate mass stars, lifetimes are computed directly from the ATON evolutionary models and range between 72.4 Myr and 1.82 Gyr for AGBs and between 41.7 and 61.7 Myr for SAGBs.

Fig. 13 shows the evolution of the total mass of dust (solid line), silicates (dashed line) and carbon grains (dotted

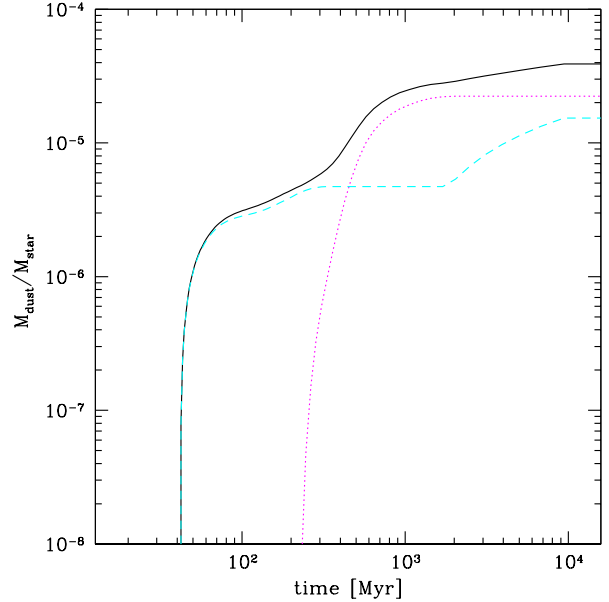


**Figure 13.** Time evolution of the mass of dust produced by AGBs/SAGBs normalized to the total mass of stars (solid line). All stars are assumed to form in a single burst at  $t = 0$  with a metallicity of  $Z = 5 \times 10^{-2} Z_{\odot}$  and a Larson IMF with  $m_{\text{ch}} = 0.35 M_{\odot}$ . The dashed and dotted lines show the separate contributions of silicates and of carbon dust, respectively.

line). All the stars are assumed to form in a single burst at  $t = 0$  with initial metallicity of  $Z = 5 \times 10^{-2} Z_{\odot}$  and the mass of dust is normalized to the total stellar mass formed.

Since massive AGBs and SAGBs stars are the most efficient silicates producers, about 50 Myr after the burst



silicates dominate the dust mass evolution. When stars of  $M \sim 3M_{\odot}$  have ended their evolution, about 300 Myr after the burst, the production of silicates ceases and restarts only when stars with  $M \leq 2M_{\odot}$  reach their AGB phase ( $\sim 1.7$  Gyr after the burst). Carbon dust enrichment is delayed to longer timescales, being produced only by stars with masses  $\leq 3M_{\odot}$ ; this represents the dominant dust component after  $\sim 470$  Myr of the burst.

Thus, if AGBs and SAGBs stars are the dominant star-dust sources, the ISM in galaxies at  $z > 10$  and in young starbursts with ages  $< [450 - 500]$  Myr at any redshift will be predominantly enriched by silicates and no carbon dust features are expected to be observable. It is clear that these findings may partially depend on the adopted initial metallicity of the stars, which affect both the core mass and the surface chemistry of the stars. In a future study, we will investigate the formation of dust using a grid of AGBs/SAGBs exploring the full range of metallicities  $0 \leq Z \leq Z_{\odot}$ .

Presence of carbon dip in the (rest-frame) UV spectrum of galaxies at  $z \sim 1-3$  (Noll et al. 2007, 2009) suggests that these host evolved (age exceeding a few hundred million years) stellar populations. The lack of carbon dip in the spectra of AGN and high redshift quasars, accompanied by the presence of the silicate feature at  $10\mu\text{m}$ , suggests that these active nuclei are hosted in young stellar populations (Maiolino et al. 2001; Lutz et al. 2008; Maiolino et al. 2004; Gallerani et al. 2010).

## 7 CONCLUSIONS

We investigate the production of dust using physical models of AGB and SAGB stars with mass in the range  $1M_{\odot} \leq M \leq 8M_{\odot}$  and initial metallicities  $Z = 0.001$ .

The type of dust formed depends on the HBB ignition at the bottom of the external mantle: HBB is accompanied by the depletion of surface carbon, which, in turn, prevents the production of carbon dust, in favour of silicates. The threshold mass above which only silicates are formed is found to be  $M = 3M_{\odot}$ . Below this limit, the evolution in the surface chemistry is dominated by TDU with the consequent formation of carbon dust.

The distribution with stellar mass of the amount of dust formed shows a minimum corresponding to the  $[3.5 - 5]M_{\odot}$  mass range due to the combined effects of the soft HBB experienced by these stars and inefficient mass loss. The strength of HBB increases with stellar mass leading to almost complete destruction of surface oxygen for stars with  $M \sim 6M_{\odot}$ ; this, in turns, limits the formation of silicates and leaves solid iron as the dominant dust species.

SAGB models are expected to produce great amounts of silicates. They experience large mass loss rates, ejecting their external envelope before significant surface oxygen depletion.

In contrast with previous studies, we show that use of the FST treatment, as in the present investigation, leads to an efficient HBB ignition in all models with masses  $M > 3M_{\odot}$ , that are thus predicted to produce silicates. This is at odds with previous results published in the literature coming from synthetic AGB models based on the MLT treatment, which predicts C-rich dust to be the dominant species at all masses.

As a consequence of the strongly mass-dependent dust composition found by our physical AGB models based on FST treatment of turbulent convection, whenever the ISM dust enrichment is dominated by AGBs and SAGBs at low metallicities, we predict an early phase ( $\sim 300$  Myr) of silicate production followed by the formation of C-rich dust.

## ACKNOWLEDGMENTS

The authors are indebted to Prof. Gail for the many helpful discussions, and for providing the data for the formation enthalpies of some of the molecules entering this treatment. MDC acknowledges financial support from the Observatory of Rome.

## REFERENCES

- Angulo C., Arnould M., Rayet M., et al., 1999, Nucl.Phys. A, 656, 3
- Bell K.R., Lin D.N.C., 1994, ApJ, 427, 987
- Blöcker T., 1995, A&A, 297, 727
- Blöcker T., Schönberner D., 1991, A&A, 244, L43
- Bowen G. H., 1988, ApJ, 329, 299
- Canuto V.M.C., Mazzitelli I., 1991, ApJ, 370, 295
- Cloutman L.D., Eoll J.G., 1976, ApJ, 206, 548
- Cristallo S., Straniero O., Lederer, M.T., Aringer B., 2008, ApJ, 667, 489
- Ferrarotti A.D., Gail H.P., 2001, A&A, 371, 133
- Ferrarotti A.D., Gail H.P., 2002, A&A, 382, 256
- Ferrarotti A.D., Gail H.P., 2006, A&A, 553, 576
- Formicola A., Imbriani G., Costantini H., et al., 2004, Phys. Lett. B, 591, 61
- Fynbo H.O.U., et al, 2005, Nature, 433, 136
- Gail H.P., Sedlmayr E., 1999, A&A, 347, 594
- Gallerani S., Maiolino R., Juarez Y., et al., 2010, A&A, 523, 85
- Grevesse N., Sauval A.J., 1998, SSRv, 85, 161
- Hale S.E., Champagne A.E., Iliadis C., et al., 2002, Phys. Rev. C, 65, 5801
- Hale S.E., Champagne A.E., Iliadis C., et al., 2004, Phys. Rev. C, 70, 5802
- Herwig F., 2000, A&A, 360, 952
- Herwig F., 2005, AR&A, 43, 435
- Herwig F., Austin S.M., 2004, ApJ, 613, L73
- Höfner S., 2009, Asp. Conf. Ser., 414, p.3
- Iben I. Jr., Renzini A., 1983, ARA&A, 21, 271
- Ivezic Z., Elitzur M., 2010, MNRAS, 404, 1415
- Karakas A.I., Lattanzio J.C., 2003, PASA, 20, 279
- Karakas A. I., Lugaro M. A., Wiescher M., Görres J., Ugalde C., 2006, ApJ, 643, 471
- Kunz R., Fey M., Jaeger M., Mayer A., Hammer J.W., Staudt G., Harissopulos S., Paradellis T., 2002, ApJ, 567, 643
- Lucy L.B., 1971, ApJ, 163, 95
- Lucy L.B., 1976, ApJ, 205, 482
- Lutz D., Sturm E., Tacconi L. J., Valiante E., Schweitzer M., Netzer H., Maiolino R., Andreani P., Shemmer O., Veilleux S., 2008, ApJ, 684, 353
- Maiolino R., Marconi A., Salvati M., Risaliti G., Severgnini P., Oliva E., La Franca, F., Vanzì L., 2001, A&A, 365, 28



- Maiolino R., Oliva E., Ghinassi F., Pedani M., Mannucci F., Mujica R., Juarez Y., 2004, *A&A*, 420, 889
- Marigo P., 2002, *A&A*, 387, 507
- Marigo P., Aringer B., 2009, *A&A*, 508, 1538
- Mattsson L., Höfner S., Herwig F., 2007, *A&A*, 470, 339
- McDonald I., Boyer M. L., van Loon J., Zijlstra A. A., 2011, *ApJ*, 730, 71
- Noll S., Pierini D., Pannella M., Savaglio S., 2007, *A&A*, 472, 455
- Noll S., Pierini D., Cimatti A., 2009, *A&A*, 499, 69
- Ossenkopf V., Henning Th., Mathis J. S., 1992, *A&A*, 261, 567
- Paczynski B., 1970, *Acta Astron.*, 20, 47
- Renzini A., Voli M., 2009, *A&A*, 94, 175
- Sackmann I. J., Smith R. L., Despain K. H., 1974, *ApJ*, 187, 555
- Siess L., 2006, *A&A*, 448, 717
- Siess L., 2010, *A&A*, 512, A10
- Sharp C.M., Huebner W.F., 1990, *ApJS*, 72, 417
- Sloan G. C., Kraemer K. E., Wood P. R., Zijlstra A. A.; Bernard-Salas J., Devost D., Houck J. R., 2008, *ApJ*, 686, 1056
- Sloan G. C., Matsuura M., Zijlstra A. A., 2009, *Science*, 323, 353
- Sloan G. C., Kraemer K. E., Bernard-Salas J., 2010a, *A&AS*, 2154, 5902
- Sloan G. C., Matsunaga N., Matsuura M., et al., 2010b, *ApJ*, 719, 1274
- Straniero O., Chieffi A., Limongi M., Busso M., Gallino R., Arlandini, C., 1997, *ApJ*, 478, 332
- Valiante R., Schneider R., Bianchi S., Andersen A., Anja C., 2009, *MNRAS*, 397, 1661
- Valiante R., Schneider R., Salvadori S., Bianchi S., 2011, *MNRAS*, in press
- Vassiliadis E., Wood P.R., 1993, *ApJ*, 413, 641
- Ventura P., D'Antona F., 2005a, *A&A*, 341, 279
- Ventura P., D'Antona F., 2005b, *A&A*, 439, 1075
- Ventura P., D'Antona F., 2008, *A&A*, 479, 805
- Ventura P., D'Antona F., 2009, *A&A*, 499, 835
- Ventura P., D'Antona F., 2011, *MNRAS*, 410, 2760
- Ventura P., Marigo P., 2009, *MNRAS*, 399, L54
- Ventura P., Marigo P., 2010, *MNRAS*, 408, 2476
- Ventura P., D'Antona F., Mazzitelli I., 2000, *A&A*, 363, 605
- Ventura P., D'Antona F., Mazzitelli I., Gratton, R., 2001, *ApJ*, 550, L65
- Ventura P., Zeppieri A., Mazzitelli I., D'Antona F., 1998, *A&A*, 334, 953
- Vitense E., 1953, *Z. Astrophys.*, 32, 135
- Woitke E., 2006, *A&A*, 460, L9
- Zhukovska S., Gail H. P., Tieloff M., 2008, *A&A*, 479, 453